THE JOURNAL OF PHYSICAL CHEMISTRY B LETTERS

2005, *109,* 23125−23128
Published on Web 11/19/2005

Synthesis of Gold Nanoparticles by Laser Ablation in Toluene: Quenching and Recovery of the Surface Plasmon Absorption

Vincenzo Amendola,[†] Gian Andrea Rizzi,[†] Stefano Polizzi,[‡] and Moreno Meneghetti*[,†]

Department of Chemical Sciences, University of Padova, Via Marzolo 1, I-35131 Padova, Italy, and Department of Physical Chemistry, University of Venezia, Via Torino 155/b, I-30172 Venezia, Italy

Received: October 11, 2005; In Final Form: November 10, 2005

Gold nanoparticles are synthesized by laser ablation of a gold plate in toluene. The nanoparticles do not show their characteristic surface plasmon absorption (SPA) and are found to be included in a graphitic matrix. The absence of this absorption is found to derive from the presence of the matrix which prevents the growth of large nanoparticles and covers them, suppressing the SPA according to the Mie model for core@shell particles. It is possible to recover the nanoparticle SPA by oxidizing the carbon matrix, obtaining, therefore, some control on the activity of this absorption.

Gold nanoparticles (AuNP) are widely studied for their properties, which find application in many different fields, from material to medical science.[1−15] A key factor in the progress of this research area is the easy availability of AuNP with controlled size and shape,[1,5,8,14,15] which can be obtained with appropriate synthesis methodologies.

Gold colloids are usually obtained by chemical reduction of gold ions.[14,16,17] However, in this type of synthesis, ligands are needed in order to control the mean radius of the particles and the reduction is limited to some type of solvents. Furthermore, the undesired components such as unreacted surfactants and other reagents have to be removed.[1]

The recent work of Mafunè et al.[18−20] on the synthesis of AuNP by laser ablation of metal plates in an aqueous solution of sodium dodecyl sulfate (SDS) opened new perspectives for the extremely simple synthesis procedure and also for particle size control. Only a limited number of other solvents, like aliphatic alcohols and alkanes, have been used for the same type of synthesis.[21,22]

We have begun the study of the synthesis of AuNP by laser ablation in organic solvents with the aim of obtaining the nanoparticles in solvents which can also solubilize organic molecules useful for functionalizing AuNP.[23]

In this letter, we show that the synthesis by laser ablation in toluene produces a very different and interesting result with respect to what is obtained with other solvents. Usually, nanometric size gold particles present a characteristic red color due to the surface plasmon absorption (SPA) near 530 nm.[1] This is what we also obtained by laser ablation in dimethyl sulfoxide (DMSO).[23] The synthesis in toluene, on the contrary, produced AuNP without the characteristic SPA.

AuNP synthesis via laser ablation in a toluene solution was conducted with a fluence of 3 J/cm^2 for 10 min using 9 ns pulses at 10 Hz of a Nd:YAG laser (Quantel YG980E) at 1064 nm. The laser beam was focused with a 10 cm focus lens to a spot of about 300 μm, on a gold plate at the bottom of a cell below about 3 cm of toluene. Solvent temperature was found to be below 40 °C at the end of the synthesis.

To the naked eye, the solution has a yellow amber color, instead of the red color characteristic of gold colloidal suspension.[1] In Figure 1a is reported the UV−vis spectrum of the toluene solution, where one can note the absence of the SPA. This is clearly different from the result obtained using other solvents under the same synthesis conditions (see Figure 1).[23]

We also used another aromatic solvent similar to toluene like benzonitrile and found the same result that was obtained with toluene, namely, the absence of the SPA (see Figure 1). This suggests the importance of a solvent like a benzene derivative for obtaining the SPA quenching. The inset of Figure 1 shows that the UV−vis spectrum of the evaporated solution on a microscopy slide has the same structure of the colloidal solution.

Figure 1b shows the micro-Raman spectrum of the nanoparticles deposited on the slide recorded with a Renishaw InVia Raman microscope and using the 488 nm line of an Ar laser.

One observes two broad peaks which are characteristic of the graphitic carbon spectrum: one at 1355 cm^{-1} (D band) and another more intense one at 1592 cm^{-1} (G band).[24,25] For comparison in Figure 1b, the spectra of graphite and carbon black are also reported. One can see that the ratio of the D band to the G band integrated intensities for our sample ($I_{DG} = 1.6$) is smaller than that of carbon black ($I_{DG} = 2.0$), indicating a larger amount of crystalline graphite. For an evaluation of the dimension of the crystals, we can use the linear relationship reported by Tuinstra et al.[26] between the reciprocal of the in-plane graphite crystal length ($1/L_a$) and the ratio of the D band to the G band integrated intensities (I_{DG}). We find that the graphite crystals present in our samples have an average size of 2.7 nm. Micro-Raman spectra of nanoparticles obtained with other solvents than toluene or benzonitrile did not show the graphitic bands.

* To whom correspondence should be addressed. E-mail: moreno.meneghetti@unipd.it.
[†] University of Padova.
[‡] University of Venezia.

10.1021/jp055783v CCC: $30.25

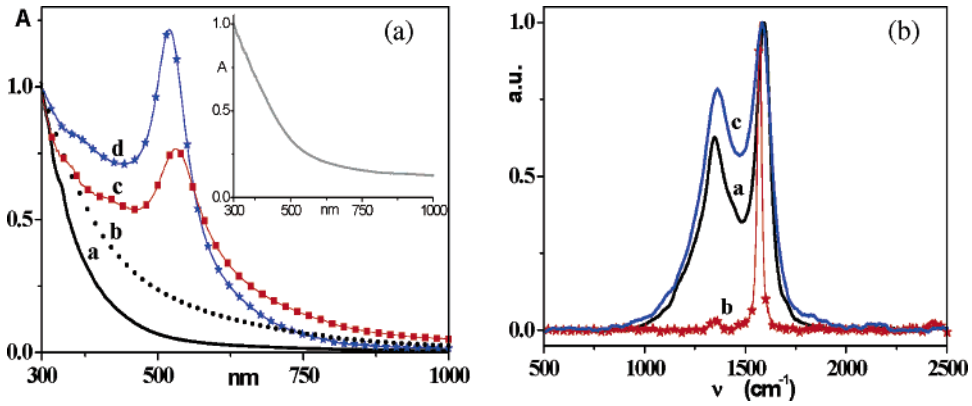

Figure 1. (a) UV−vis spectra of AuNP solutions obtained by laser ablation in toluene (curve a, black line), in benzonitrile (curve b, dotted line), and, for comparison, in DMSO (curve c, red squares) and in water (curve d, blue stars). Inset: AuNP obtained in toluene evaporated on a microscopy slide. All spectra are normalized at 300 nm. (b) Raman spectra (exciting line at 488 nm) of AuNP deposited on the microscopy slide (curve a, black line). Graphite (curve b, red stars) and carbon black (curve c, blue line) spectra are reported for comparison. All spectra are normalized with respect to the G band peak.

X-ray photoelectron spectroscopy (XPS) analysis confirmed the result obtained with the Raman spectra. A custom-made ultrahigh vacuum chamber equipped with an EA125 Omicron analyzer and an Al Kα source and an operating pressure of 10^{-9} mbar have been used for the XPS measurements. The XPS spectrum shows a strong carbon 1s peak centered at 284.0 eV which confirms the presence of graphitic carbon, whereas a tail toward higher binding energies shows that amorphous carbon is also present. Furthermore, we observed a doublet at 83.7 and 87.4 eV, as expected, corresponding to the gold $4f_{7/2}$ and $4f_{5/2}$ doublet. Since the ratio of C 1s to Au 4f peak integrated intensities is 12:1, one can deduce that carbon is present in a large amount.

We also recorded transmission electron microscopy (TEM) images at 300 kV with a JEOL JEM 3010 microscope equipped with a Gatan Multiscan CCD camera, model 794. Samples were prepared by evaporating the solutions on a copper grid covered with an amorphous carbon holey film. The TEM image reported in Figure 2a shows AuNP surrounded by graphitic nanocrystals with sizes variable among nanometer fractions to tens of nanometers, in agreement with the estimation made with the Tuinstra relationship. These nanocrystals show well-defined planes and are present in remarkable concentration around AuNP. The interplanar distance of such crystals corresponds to the 3.4 Å value of bulk graphite along the *c* axis direction (inset of Figure 2a). Around small nanoparticles, graphite crystals are not clearly observed, but the contours of these particles are not well-defined. This suggests their inclusion in an amorphous carbon matrix which also prevents their growing, although the interparticle distance is very small. A statistical analysis on more than 1000 AuNP shows that they have an average radius of only 0.9 nm, with a standard deviation of ±0.5 nm.

The graphitic carbon matrix formation can be explained by recalling that the synthesis of graphitic materials based on the pyrolysis of benzene is reported in the literature.[27,28] We can deduce that the process which produces graphitic structures around AuNP in our samples is of the same nature, since we measured a Raman spectrum very similar to that reported for the graphitic materials obtained by benzene pyrolysis.[29]

It was experimentally shown that, for very small AuNP, with a radius below 1.0 nm, the SPA is almost vanishing.[19,30,31] Since the distribution of the particles we obtained (see Figure 2b) shows that almost 70% of the particles have a radius below 1.0 nm, quenching of the SPA can be explained considering that

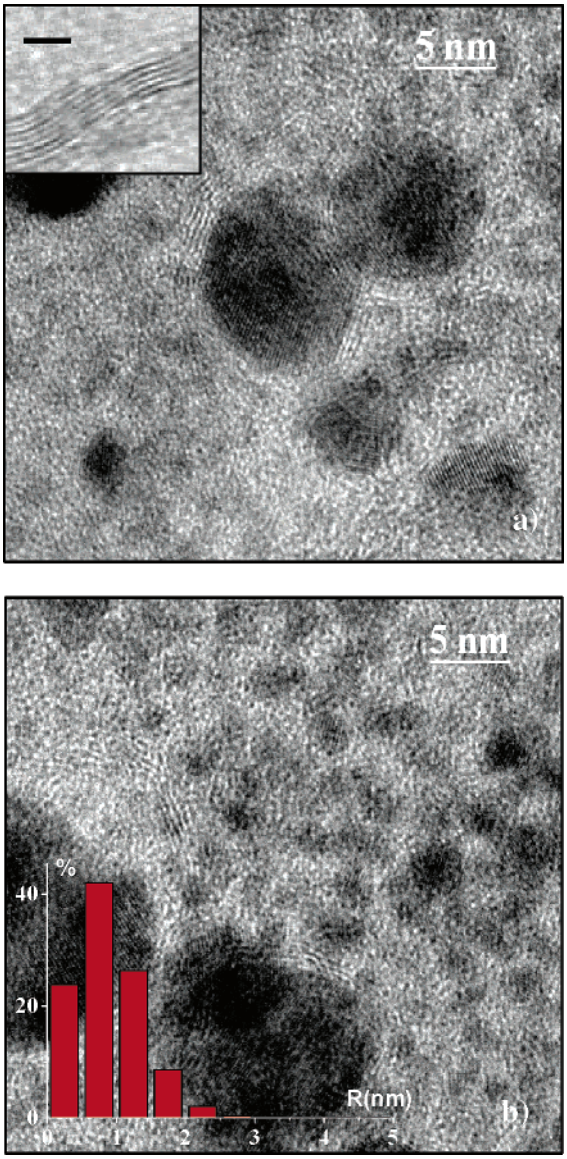

Figure 2. TEM images of AuNP included in a graphitic carbon matrix. (a) Planes of graphitic nanostructures surrounding AuNP; the inset shows a magnification of such a nanostructure, where an interplanar distance of 0.34 nm can be appreciated (bar = 2 nm). (b) Distribution of AuNP in the carbon matrix; the inset shows a radius distribution of more than 1000 AuNP.

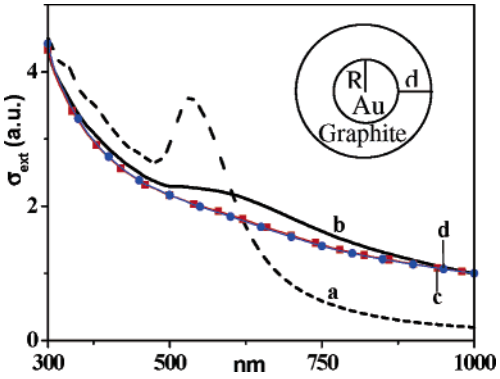

Figure 3. SPA calculated with the Mie model for a compact gold sphere with a radius of $R = 1.0$ nm (curve a, dashed line) and for a core@shell sphere with a Au core radius of $R = 1.5$ nm and a graphite shell thickness of $d = 1.5$ nm (curve b, black line), $d = 3.75$ nm (curve c, red squares), and $d = 5.0$ nm (curve d, blue circles). In all calculations, toluene is the external medium.

the carbon matrix precludes the formation of larger particles and therefore, indirectly, the presence of the SPA. However, 30% of the particles have radii which are larger than 1.0 nm and therefore they should show a clear SPA,[30] which is not observed. Mie theory[32] can help create an understanding of this phenomenon.

To take into account the influence of the carbon matrix on the extinction cross section (σ_{ext}), we use the Mie theory extension for core@shell spheres, considering that carbon is a shell around Au nanoparticles with a radius of 1.5 nm (see inset of Figure 3).[33] In the quasi-static regime, we can use the following dipolar approximation for the polarizability ($\alpha(\omega)$) of the core@shell sphere: [33]

$$\alpha(\omega) = \frac{4\pi}{3}(R + d)^3\epsilon_0\frac{(\epsilon_s - \epsilon_m)(\epsilon + 2\epsilon_m) + \left(\frac{R}{R+d}\right)^3(\epsilon - \epsilon_s)(\epsilon_m + 2\epsilon_s)}{(\epsilon_s + 2\epsilon_m)(\epsilon + 2\epsilon_s) + \left(\frac{R}{R+d}\right)^3(\epsilon - \epsilon_s)(2\epsilon_s - \epsilon_m)} \quad (1)$$

where d is the shell thickness, R is the core radius, ϵ_0 is the vacuum permittivity, ϵ_s is the shell complex dielectric function, ϵ is the core complex dielectric function, and ϵ_m is the embedding medium real dielectric function. σ_{ext} can be obtained from α according to

$$\sigma_{ext}(\omega) = 4\pi\, k\, \mathrm{Im}[\alpha(\omega)] \quad (2)$$

where k is the wavenumber of the electromagnetic radiation.

For the shell dielectric function (ϵ_s), we use the ordinary component of the graphite,[34] whereas, for the AuNP, we used the following expression:

$$\epsilon(\omega,R) = \left\{\epsilon_{1\infty}(\omega) + \omega_P^2\left(\frac{1}{\omega^2 + \Gamma_\infty^2} - \frac{1}{\omega^2 + \Gamma(R)^2}\right)\right\} + i\left\{\epsilon_{2\infty}(\omega) + \frac{\omega_P^2}{\omega}\left(\frac{\Gamma(R)}{\omega^2 + \Gamma(R)^2} - \frac{\Gamma_\infty}{\omega^2 + \Gamma_\infty^2}\right)\right\} \quad (3)$$

where Γ_∞ is the relaxation constant for the bulk metal, ω_P is the plasma frequency, and $\epsilon_{1\infty}(\omega)$ and $\epsilon_{2\infty}(\omega)$ are real and imaginary components of the bulk metal dielectric function.[35] The dependence on R is introduced through the size dependent

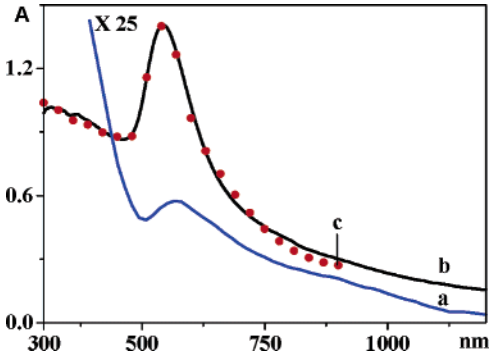

Figure 4. UV−vis spectra of the nanocomposite after oxidation in solution (curve a, blue line; magnification ×25) and after thermal treatment (curve b, black line). Mie fitting of the annealed sample in air is reported as filled red circles (curve c).

electronic relaxation constant ($\Gamma(R)$), which can be expressed as[33]

$$\Gamma(R) = \Gamma_\infty + A\frac{\upsilon_F}{R} \quad (4)$$

where υ_F is the Fermi speed and A is a constant with a value near 1.

Figure 3 shows that the SPA is strongly suppressed for $d = R = 1.5$ nm and that for $d = 3.75$ nm it is completely suppressed. Therefore, the SPA quenching is obtained for a value of d which is in agreement with TEM images and with the value for the dimension of crystallites (2.7 nm) obtained with the Tuinstra relationship (see above). This shows, therefore, that the carbon matrix has not only the role of controlling the growth of the nanoparticles but also that of suppressing the SPA of larger nanoparticles.

According to Mie theory results, a recovery of AuNP SPA can be obtained by removing the carbon matrix. We have obtained this result both for the colloidal solution and for the solid nanocomposite by oxidizing the carbon matrix.

For the colloidal solution, we adopted the following procedure: The AuNP solution was evaporated to remove toluene; then, the residue was resolubilized in a 4:1 mixture of a 96% solution of H_2SO_4 and a 30% solution of H_2O_2. The solution was kept at 70 °C overnight. Figure 4 reports the UV−vis spectrum of the solution after the oxidation, where a weak but clear SPA near 560 nm can be observed. The spectrum shows a SPA frequency characteristic of aggregated nanoparticles, although a fitting with the Mie model is difficult to obtain due to its weakness and to the presence of the absorptions of other compounds such as residual carbon particles.

We obtained better results for the solid nanocomposite. In this case, we oxidized, in air at 525 °C, the composite deposited on a microscopy slide using a tubular furnace model Carbolite MTF 10/25/130.

Figure 4 reports UV−vis spectra after 90 min of oxidation. One can clearly see the recovery of a sharp SPA at 545 nm. Fitting of these data can be obtained by using Mie theory and its extension for ellipsoidal particles.[33] The fitting (see Figure 4) indicates the presence of 65.5% nanospheres with a radius of 32.5 nm and of 34.5% nanospheroids, namely, ellipsoidal particles with two principal axes, adopting for their aspect ratio a narrow Gaussian distribution with a standard deviation of 1.1. The remarkable increase of the average radius and the spheroid fraction indicates that, by removing the graphitic carbon matrix, the AuNP show large aggregation and growth which allow the recovery of the AuNP SPA.

The micro-Raman spectrum after the thermal treatment shows the complete disappearance of both D and G bands. Also, the XPS spectrum shows that the 1s graphitic carbon peak at 284.0 eV disappears and only a very weak peak at 284.7 eV remains, with a relative intensity of 0.125:1 with respect to the Au 4f doublet, against the value of 12:1 observed before the treatment.

We observed a different result using a thermal treatment of the nanocomposite in a N_2 atmosphere for 3 h at 525 °C. In this case, the carbon matrix is not removed but, on the contrary, the matrix graphitization was promoted. The micro-Raman spectrum recorded after this treatment shows a decrease of the intensity of the D band with respect to the G one. The ratio of the integrated intensity of these bands (I_{DG}) changed from 1.6 to 1.0, and applying the Tuinstra relationship, this indicates that the graphite particles have an average in-plane length of 4.7 nm. The UV−vis spectrum of the nanoparticles, obtained after the treatment, does not show any SPA, as expected.

Composites of graphite and AuNP have been considered interesting for sensors,[36,37] and the present synthesis approach can be a simple way for obtaining such materials.

In conclusion, we have shown that AuNP can be obtained by laser ablation in a toluene solution. The as-grown nanoparticles are included in a graphitic carbon matrix which limits their growth and aggregation and causes the quenching of the SPA characteristic of AuNP. The graphitic shell was removed by chemical oxidation of the nanoparticles in solution and by thermal treatment in air of the deposited nanocomposite. In both cases, the SPA was recovered. The analysis of the UV−vis spectra with the Mie models shows that AuNP aggregate both in solution and in the deposited nanocomposite. Thermal treatment of the nanocomposite in a N_2 atmosphere produced a nanocomposite material with larger graphite crystals.

Acknowledgment. The authors would like to thank MIUR for financial support (FIRB funding program n. RBNE01P4JF).

References and Notes

(1) Daniel, M. C.; Astruc, D. *Chem. Rev.* **2004**, *104*, 293−346.
(2) Hutter, E.; Fendler, J. H. *Adv. Mater.* **2004**, *16*, 1685−1706.
(3) Kamat, P. V. *J. Phys. Chem. B* **2002**, *106*, 7729−7744.
(4) Henglein, A. *J. Phys. Chem.* **1993**, *97*, 5457−5471.
(5) Feldheim, D. L.; Keating, C. D. *Chem. Soc. Rev.* **1998**, *27*, 1−12.
(6) Gittins, D. I.; Bethell, D.; Schiffrin, D. J.; Nichols, R. J. *Nature* **2000**, *408*, 67−69.
(7) Schneider, B. H.; Dickinson, E. L.; Vach, M. D.; Hoijer, J. V.; Howard, L. V. *Biosens. Bioelectron.* **2000**, *15*, 597−604.
(8) Boyer, D.; Tamarat, P.; Maali, A.; Lounis, B.; Orrit, M. *Science* **2002**, *297*, 1160−1163.
(9) Talley, C. E.; Jackson, J. B.; Oubre, C.; Grady, N. K.; Hollars, C. W.; Lane, S. M.; Huser, T. R.; Nordlander, P.; Halas, N. J. *Nano Lett.* **2005**, *5*, 1569−1574.
(10) Yelin, D.; Oron, D.; Thiberge, S.; Moses, E.; Silberberg, Y. *Opt. Express* **2003**, *11*, 1385−1391.
(11) Nam, J. M.; Thaxton, C. S.; Mirkin, C. A. *Science* **2003**, *301*, 1884−1886.
(12) Jackson, A. M.; Myerson, J. W.; Stellacci, F. *Nat. Mater.* **2004**, *3*, 330−336.
(13) Yu, A.; Liang, Z.; Cho, J.; Caruso, F. *Nano Lett.* **2003**, *3*, 1203−1207.
(14) Xia, Y.; Halas, N. J. *MRS Bull.* **2005**, *30*, 5.
(15) Gunnarsson, L.; Rindzevicius, T.; Prikulis, J.; Kasemo, B.; Kall, M.; Zou, S. L.; Schatz, G. C. *J. Phys. Chem. B* **2005**, *109*, 1079−1087.
(16) Watson, K. J.; Zhu, J.; Nguyen, S. B. T.; Mirkin, C. A. *J. Am. Chem. Soc.* **1999**, *121*, 462−463.
(17) Jana, N. R.; Gearheart, L.; Murphy, C. J. *J. Phys. Chem. B* **2001**, *105*, 4065−4067.
(18) Mafune, F.; Kohno, J.; Takeda, Y.; Kondow, T.; Sawabe, H. *J. Phys. Chem. B* **2001**, *105*, 5114−5120.
(19) Mafune, F.; Kohno, J. Y.; Takeda, Y.; Kondow, T. *J. Phys. Chem. B* **2002**, *106*, 7575−7577.
(20) Mafune, F.; Kondow, T. *Chem. Phys. Lett.* **2003**, *372*, 199−204.
(21) Compagnini, G.; Scalisi, A. A.; Puglisi, O.; Spinella, C. *J. Mater. Res.* **2004**, *19*, 2795−2798.
(22) Compagnini, G.; Scalisi, A. A.; Puglisi, O. *J. Appl. Phys.* **2003**, *94*, 7874−7877.
(23) Amendola, V.; Mattei, G.; Cusan, C.; Prato, M.; Meneghetti, M. *Synt. Met.*, in press.
(24) Matthews, M. J.; Pimenta, M. A.; Dresselhaus, G.; Dresselhaus, M. S.; Endo, M. *Phys. Rev. B* **1999**, *59*, 6585−6588.
(25) Wang, Y.; Alsmeyer, D. C.; Mccreery, R. L. *Chem. Mater.* **1990**, *2*, 557−563.
(26) Tuinstra, F.; Koenig, J. L. *J. Chem. Phys.* **1970**, *53*, 1126−1130.
(27) Koyama, T. *Carbon* **1972**, *10*, 757−765.
(28) Koyama, T.; Endo, M.; Onuma, Y. *Jpn. J. Appl. Phys.* **1972**, *11*, 445−449.
(29) Chieu, T. C.; Dresselhaus, M. S.; Endo, M. *Phys. Rev. B* **1982**, *26*, 5867−5877.
(30) Alvarez, M. M.; Khoury, J. T.; Schaaff, T. G.; Shafigullin, M. N.; Vezmar, I.; Whetten, R. *J. Phys. Chem. B* **1997**, *101*, 3706−3712.
(31) Subramanian, V.; Wolf, E. E.; Kamat, P. V. *J. Am. Chem. Soc.* **2004**, *126*, 4943−4950. Peng, Z.; Walther, T.; Kleinermanns, K. *J. Phys. Chem. B* **2005**, *109*, 15735−15740.
(32) Mie, G. *Ann. Phys.* **1908**, *25*, 377.
(33) Kreibig, U.; Vollmer, M. *Optical Properties of Metal Clusters*; Springer-Verlag: Berlin, 1995.
(34) Borghesi, A.; Guizzetti, G. *Handbook of Optical Constants of Solids II*; Academic: Boston, MA, 1991.
(35) Johnson, P. B.; Christy, R. W. *Phys. Rev. B* **1972**, *6*, 4370−4379.
(36) Simm, A. O.; Banks, C. E.; Wilkins, S. J.; Karousos, N. G.; Davis, J.; Compton, R. G. *Anal. Bioanal. Chem.* **2005**, *381*, 979−985.
(37) Biswas, P. C.; Nodasaka, Y.; Enyo, M.; Haruta, M. *J. Electroanal. Chem.* **1995**, *381*, 167−177.